Journal of Southeast University (English Edition) Vol. 39, No. 1, pp. 74 - 80 Mar. 2023 ISSN 1003—7985

Analysis of pole-slot combination of novel flux-adjustable permanent magnet adjustable speed drive with fixed air-gap

Li Yibo[1] Huang Jiacai[1] Zhu Zhiying[2]

([1]Industrial Center/School of Innovation and Entrepreneurship, Nanjing Institute of Technology, Nanjing 211167, China)
([2]School of Electric Power Engineering, Nanjing Institute of Technology, Nanjing 211167, China)

Abstract: To further improve the output torque of a permanent magnet adjustable speed drive (PMASD) and simplify the mechanical operation mechanism required in the speed regulation process, a flux-adjustable PMASD with a fixed air-gap is proposed by combining the slotted conductor rotor (CR) structure with the mechanical flux adjustment method. First, the structural characteristics and operating principle of the proposed PMASD are described. Then, the key factors affecting its basic electromagnetic characteristics are analyzed based on a theoretical model and the finite element method. The combination between the number of permanent magnet poles and the number of CR slots is mainly studied. Finally, the optimal pole-slot matching scheme was obtained with the goal of the maximum output torque and minimum torque ripple, and the principle prototype was manufactured to obtain its speed regulation characteristics, power, loss, and efficiency. The analysis results are verified comprehensively. The results show that the torque ripple is large when the slot number per pole pair is even, whereas it is smaller when the slot number per pole pair is odd. Moreover, the torque ripple decreases with the increase in the slot number per pole pair.

Key words: permanent magnet adjustable speed drive; pole-slot combination; analytical model; finite element method; squirrel cage rotor; torque characteristics

DOI: 10.3969/j.issn.1003-7985.2023.01.009

The electric energy consumption of electric motors accounts for approximately 60% of the total electric energy consumption in China, whereas 40.7% of these can realize energy saving through speed regulation. The energy-saving potential of a large-capacity motor drive system is huge, and it is very beneficial to realize the national strategic goal of energy saving and emission reduction[1-2]. In recent years, speed regulation technology based on a permanent magnet adjustable speed drive (PMASD) has become a novel technology based on asynchronous torque transmission. The novel speed regulation technology is very beneficial to energy saving for large-capacity motor drive systems with pumps and fan loads, which can realize the load speed regulation with an almost-constant prime mover speed[3-5]. The energy input of a prime mover can be greatly reduced due to the wide speed regulation range, and then the system efficiency can be improved correspondingly. Compared with the speed regulation technology based on the large-capacity and high-voltage variable-frequency drive, the application of a PMASD can avoid the problems of high harmonic pollution of the power grid and the high cost of manufacturing and maintenance[6]. Compared with a hydraulic speed regulating coupler and electromagnetic slip coupler, PMASDs can save occupied space, and, more importantly, they can also improve the torque transmission capacity and the stability and reliability of the equipment operation[7-9]. The new speed regulation technology based on a PMASD has a low cost, small size, convenient maintenance, and strong adaptability to harsh environments. Thus, it is favored by many industrial and mining enterprises.

A PMASD with a slotted conductor rotor (CR) was investigated to improve the torque density of PMASDs, and its air-gap magnetic field and transient characteristics were deeply analyzed and studied. Then, the effects of the slot and teeth on the air-gap magnetic field, induced by the eddy current of the CR and output torque, were considered comprehensively[10-11]. A PMASD with a non-rotating mechanical flux adjuster (MFA) is proposed in the previous research of the author, and its air-gap flux can be flexibly regulated by the MFA shifting control, which is beneficial to realize the regulation of the speed and torque on the load side[12]. In summary, the above scheme greatly simplifies the mechanical operation mechanism used to translate the high-speed rotors of the traditional PMASD.

The novel PMASD is proposed based on the idea of replacing a non-slotted CR with a slotted CR adopting the squirrel cage structure[12]. First, the structure characteristics and operation principle of the proposed PMASD were clearly described. Then, the key factors affecting the

Received 2022-08-04, **Revised** 2023-01-10.

Biography: Li Yibo (1989—), male, doctor, lecturer, ybli@njit.edu.cn.

Foundation items: The National Natural Science Foundation of China (No. 52107048), Jiangsu Provincial Natural Science Foundation of Higher Education (No. 21KJB470021), the Scientific Research Foundation for the High-level Personnel of Nanjing Institute of Technology (No. YKJ2019107).

Citation: Li Yibo, Huang Jiacai, Zhu Zhiying. Analysis of pole-slot combination of novel flux-adjustable permanent magnet adjustable speed drive with fixed air-gap[J]. Journal of Southeast University (English Edition), 2023, 39(1): 74 - 80. DOI: 10.3969/j.issn.1003-7985.2023.01.009.

equivalent circuit and basic electromagnetic characteristics of the PMASD were analyzed based on the theoretical model. The finite element analysis (FEA) models of the drive with different pole-slot combinations were established, and then the accurate torque characteristics and torque ripples were obtained. Finally, the optimal pole-slot combination was obtained with the goal of the maximum output torque and minimum torque ripple, and a prototype was manufactured to perform experimental tests and verify the theoretical and simulation analysis results.

1 Structure and Principle

The structure of the proposed PMASD is shown in Fig. 1, which can significantly improve the torque density and simplify the design of the mechanical operating mechanism as compared with the traditional PMASD. The proposed PMASD consists of a coaxial non-rotating mechanical MFA, an interior-mounted PMR, and a slotted CR with a copper squirrel cage. The axial position and radial length of the internal air-gap between the PMR and CR remained unchanged, and the length of the outer air-gap between the PMR and MFA was also fixed. However, the MFA can be shifted along the axial direction as needed. The PMR connected to the output shaft was arranged by spoke PMs, and the CR connected to the input shaft consisted of a copper squirrel cage embedded in a slotted CR core. In addition, all the core parts were laminated with silicon steel sheets to facilitate the manufacturing of the cores, which improved the magnetic conductivity and reduced the core losses.

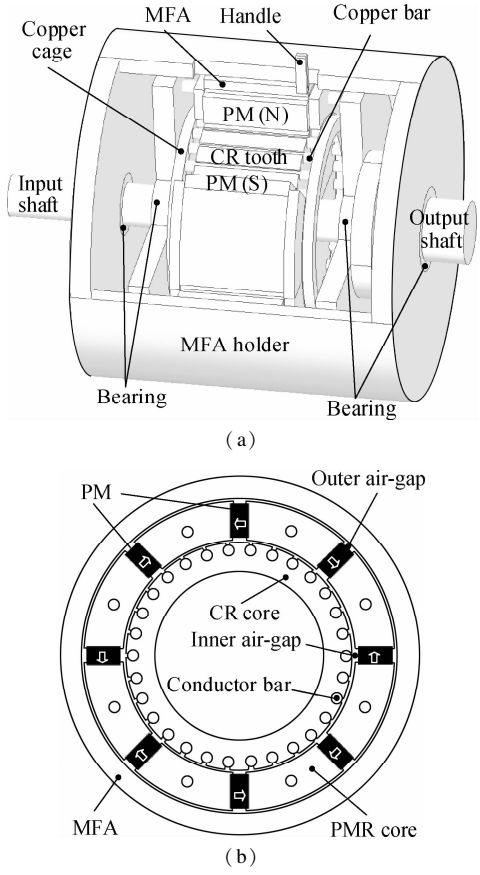

Fig. 1 Structure of the proposed PMASD. (a) Three-dimensional view; (b) Shaft section view

The flux passing through the MFA decreased with the increase in the MFA shifting distance, and then, the flux looped with the CR increased due to the almost-constant MMF of PM poles. The MFA shifting distance is the distance between the edges of the PMR and MFA along the positive direction of the MFA shifting, which can be denoted as l_{sd}. This indicates that the inner air-gap magnetic field can be flexibly adjusted by changing the coupling area between the MFA and PMR through the MFA shifting control. Based on the principle of asynchronous torque transmission, the slip speed between the two rotors can be regulated when the inner air-gap magnetic field is adjusted under a given load.

2 Theoretical Model

A theoretical model was established to make the initial design and characteristic evaluation of the PMASD more efficient. In addition, a higher torque density and lower torque ripple will be obtained by a suitable pole-slot combination. Moreover, the reliability and stability of the whole speed regulating system can be significantly improved.

Based on the equivalent magnetic circuit method, the inner air-gap flux density of the proposed PMASD can be expressed as[13-14]

$$B(\theta) = \mu_0 F_m(\theta) \Lambda(\theta) \tag{1}$$

where θ, μ_0, and $\Lambda(\theta)$ are the electrical position angle in the radian along the circumferential direction, vacuum permeability, and air-gap permeance, respectively; $F_m(\theta)$ is the magnetomotive force (MMF) in the inner air-gap, which can be expanded as a Fourier series in $[0, 2\tau_p]$ as follows[13-14]:

$$F_m(\theta) = \sum_{k=1,3,5,\cdots}^{+\infty} b_k \sin(kp\theta) \tag{2}$$

where τ_p, k, p, and b_k are the pole pitch, positive integer, pole pair number, and coefficients of the Fourier series of the MMF. In addition, the air-gap permeance can be given as[13-14]

$$\Lambda(\theta) = \frac{1}{\delta_{PMR}(\theta) + l_g + \delta_{SCR}(\theta)} \tag{3}$$

where l_g is the inner air-gap length; $\delta_{PMR}(\theta)$ and $\delta_{SCR}(\theta)$ are the additional air-gap lengths at the PMR and CR sides.

In practice, the CR of the PMASD is usually connected to the output shaft of a prime mover, whereas the PMR of the proposed drive is usually connected to a pump or fan load. Hence, the load speed is always lower than the input speed. The slip frequency between the PMR and CR can be deduced as

$$f_s = \frac{sn_{in}p}{60} \tag{4}$$

where s and n_{in} are the slip ratio between the PMR and CR and the input speed from the prime mover side, respectively. According to Faraday's law of electromagnetic induction, the MMF on the conductor bar of the squirrel-cage can be expressed as

$$E_B(\theta) = 2\pi f_s r_s B_r(\theta) l_{ef} \tag{5}$$

where r_s, $B_r(\theta)$, and l_{ef} are the center radius of the CR slot, air-gap flux density under the load state, and effective length of the conductor bar, respectively. The relationship between the effective current in the conductor bar (I_B) and the current in the end ring of each phase (I_R) can be given as[13-14]

$$I_B = 2I_R \sin\frac{\alpha_2}{2} \tag{6}$$

where α_2 is the phase difference in the electric angle between two adjacent conductor bars. Therefore, the copper loss of the whole cage can be expressed as[13-14]

$$p_{cu} = N_s(I_B^2 R_B + I_R^2 R_R) = N_s I_B^2\left[R_B + \frac{R_R}{2\sin^2(\alpha_2/2)}\right] = N_s I_B^2 R_{B+R} \tag{7}$$

where N_s, R_B, R_R, and R_{B+R} are the slot number of the CR, the resistance of the conductor bar in the CR, the phase resistance of the end ring of the squirrel cage, and the equivalent phase resistance of the whole squirrel cage, respectively.

According to the law of conservation of energy, the input mechanical power P_{in} of the proposed PMASD is mainly converted into the output mechanical power P_{out} and slip power P_s. P_{in} and P_{out} can be expressed as

$$P_{in} = T_{in}\Omega_{in} \tag{8}$$

$$P_{out} = T_{out}(1-s)\Omega_{in} \tag{9}$$

where Ω_{in}, T_{in}, and T_{out} are the input speed, input torque, and output torque, respectively, and they are almost equal to one another. From the other point of view, P_s is equal to the total copper loss of the slotted CR in ideal conditions, which is emitted in the form of heat energy. Therefore, T_{out} can be expressed as

$$T_{out} = \frac{p_{Cu}}{s\Omega_{in}} \tag{10}$$

The cogging torque of the proposed PMASD is defined as the negative derivative of the magnetic coenergy relative to the rotor position angle, which can be expressed as[15-16]

$$T_{cog}(\alpha) = -\frac{\pi l_{ef}}{4\mu_0}(r_2^2 - r_1^2)\sum_{n=1}^{\infty} nN_L\left[G_{a_nN_L}B_{a_nN_L}\sin(nN_L\alpha)\right] \tag{11}$$

where r_1 and r_2 are the internal and external radii of the inner air-gap, respectively. $G_{a_nN_L}$ and $B_{a_nN_L}$ are the Fourier coefficients. N_L is the least common multiple of the CR slot number and pole pair number in the PMR. According to Eq. (11), the number of cogging torque cycles can be expressed as

$$N_{cog} = \mathrm{LCM}(N_s, 2p) \tag{12}$$

According to Eqs. (8) to (10), the efficiency of the coupling can be expressed as

$$\eta = \frac{P_{out}}{P_{in}} = (1-s) \times 100\% \tag{13}$$

Ignoring the stray losses and mechanical loss, the input power of the proposed PMASD can be given as

$$P_{in} = (1-s)^2 P_N \tag{14}$$

where P_N denotes the rated power of the pump and fan loads. With the increase in the slip, P_{in} significantly decreases. Hence, the energy-saving effect of the system is still more pronounced than those controlled by throttling valves and baffles[4].

3 FEA Results and Discussion

In the design of the structural parameters of the PMR, the PM volume per pole changes with the variation of p when the total PM volume is given as a constant. Thus, the radial length of the PM should be adjusted with the variation of p when the PM thickness along the magnetizing direction keeps unchanged. In the design of the structural parameters of the CR, the radius of the conductor bar should be regulated with the variation of p and the CR slot number per pole pair of the PMR (N_{sp}) when the total copper volume used in the conductor bars keeps unchanged. The size of the end ring of the copper squirrel cage is kept uniform for all FEA models. Therefore, the resistance of the conductor bar and end ring between the adjacent bars will be changed according to the change in N_{sp} and p.

With the help of finite element software, the magnetic field distribution is shown in Fig. 2, where l_{sd} is 0, 25, and 50 mm. The amplitude of $B(\theta)$ increases from 0.3 to 0.7 T when l_{sd} increases from 0 to 50 mm, which is not on the same level along the axial direction. However, the flux passing through the CR increases step by step during the MFA shifting along the axial direction.

The torque slip characteristics and torque ripple T_{ripple} of the proposed PMASD are shown in Figs. 3(a) and (b), respectively. T_{out} rapidly increases with the increase in the slip s and then declines after reaching the maximum value. T_{out} increases with the increase in N_{sp}, while its variation amplitude gradually decreases. The reason is that the effective flux between the PMR and CR gradually increases

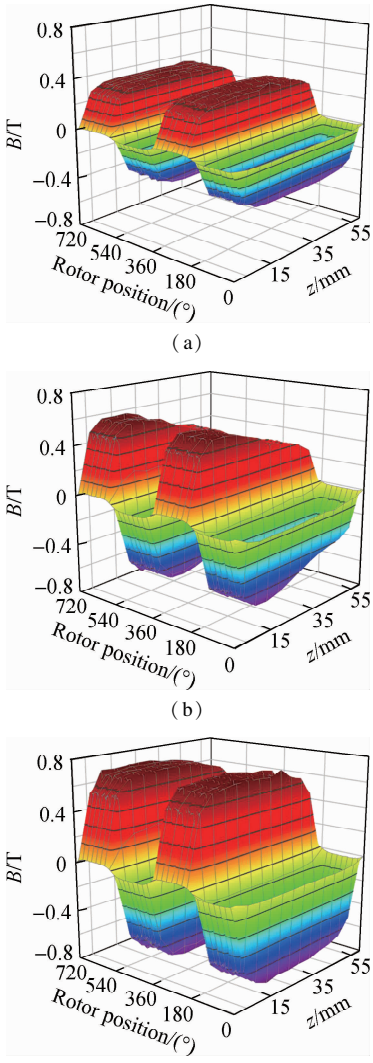

Fig. 2 Magnetic field calculation with different MFA shifting distances. (a) l_{sd} = 0 mm; (b) l_{sd} = 25 mm; (c) l_{sd} = 50 mm

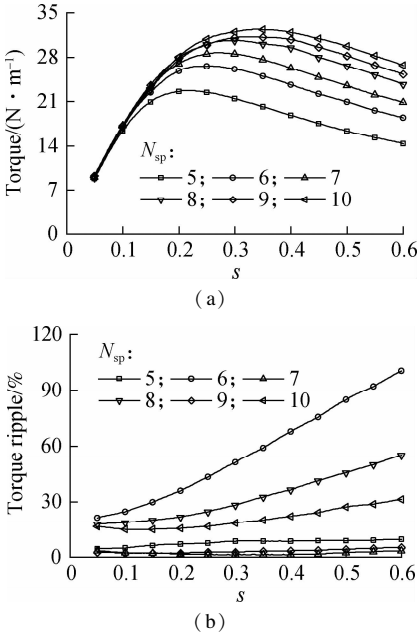

Fig. 3 Torque characteristics of the proposed PMASD (p = 4). (a) Torque slip; (b) Torque ripple

with the increase in N_{sp}. Then, the local saturation caused by the reduced CR tooth width will occur with the further increase in N_{sp}, which reduces the growth rate of the effective coupling flux. Fig. 3(b) shows that T_{ripple} increases with the increase in s, and T_{ripple} is lower than 10% when s is less than 0.6 and N_{sp} is 5, 7, and 9. In particular, T_{ripple} reaches the minimum value when N_{sp} is 7. T_{ripple} successively decreases when N_{sp} is 6, 8, and 10, and it achieves the maximum value when N_{sp} is 6. T_{ripple} is large when N_{sp} is an even value, and it gradually decreases with the increase in the even N_{sp}. However, T_{ripple} is smaller when N_{sp} is an odd value, and it declines with the increase in the odd N_{sp} in a finite interval.

Figs. 4-7 show the torque and torque ripple of the proposed PMASD with different pole-slot combinations. As

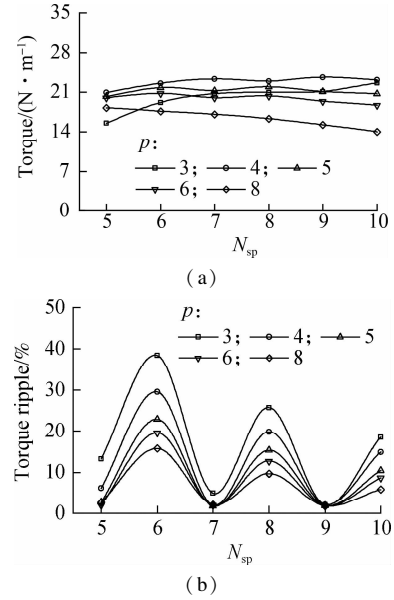

Fig. 4 Torque characteristics of the proposed PMASD (s = 0.15). (a) Torque; (b) Torque ripple

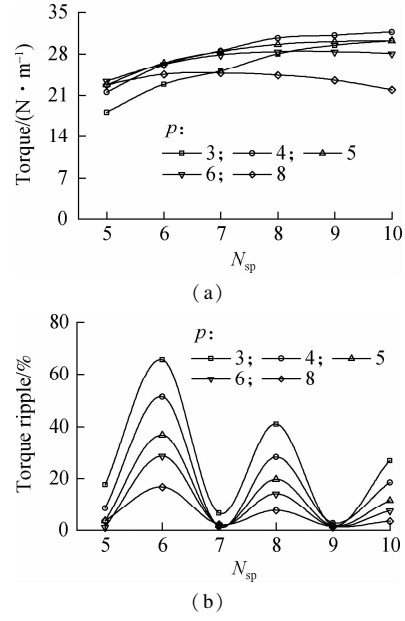

Fig. 5 Torque characteristics of the proposed PMASD (s = 0.30). (a) Torque; (b) Torque ripple

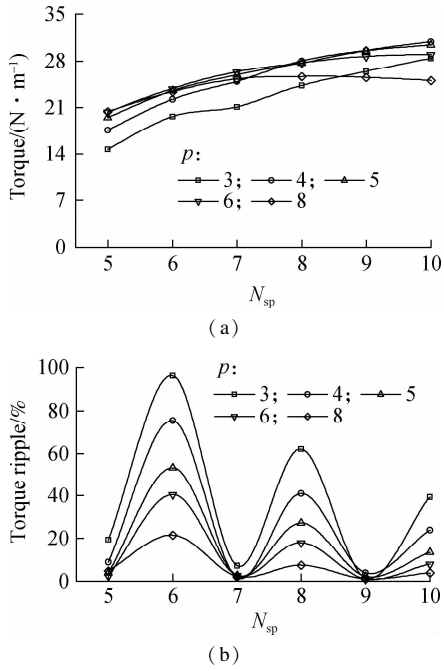

Fig. 6 Torque characteristics of the proposed PMASD (s = 0.45). (a) Torque; (b) Torque ripple

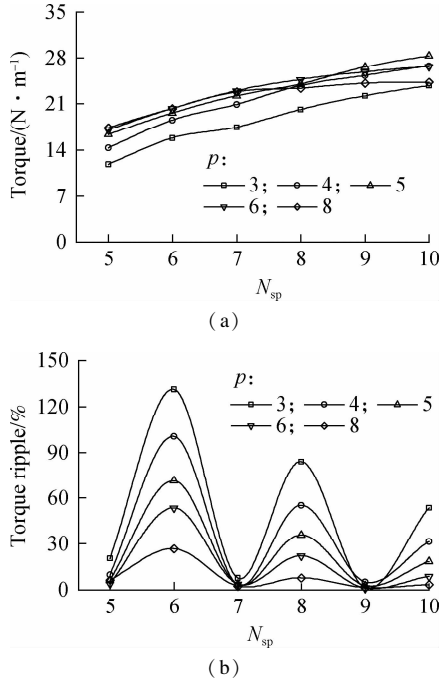

Fig. 7 Torque characteristics of the proposed PMASD (s = 0.60). (a) Torque; (b) Torque ripple

shown in Fig. 4(a), T_{out} slightly increases with the increase in N_{sp}, and the increased amplitude of T_{out} gradually declines with the increase in p. T_{out} remains almost stable with the increase in N_{sp} when p is 5, while T_{out} begins to decrease with the further increase in p. The reason is that N_s increases with the increase in p when N_{sp} is given as a constant value, and the core teeth of the CR appear saturated, which results in the weakening of the air-gap magnetic field. However, T_{ripple} is small when N_{sp} is an odd value, and it declines with the increase in N_{sp}. Figs. 4-7 show that the torque capability of the proposed PMASD is the strongest when p is 4, and T_{ripple} is approximately 3% when N_{sp} is 7 and 9.

To achieve optimal N_s when the pole pair number is 4, the variation of the torque and torque ripple is studied when N_{sp} increases from 7 to 9; that is, N_s increases from 28 to 36. As shown in Fig. 8(a), the output T_{out} remains stable with the increase in N_s. T_{out} obtains the largest value when s is 0.3, and it slightly rises with the increase in N_s when s is greater than 0.3. The reason is that the current on conductor bars gradually increases with the increase in s. Then, the induced magnetic field is enhanced with the further increase in s, which leads to the weakness of the resultant air-gap magnetic fields. T_{ripple} with different slips are shown in Fig. 8(b), which is significantly larger when N_s are 28, 32, and 36, and it obtains the largest value when N_s is 32. T_{ripple} is smaller, and its values show a little difference when N_s is 29, 30, 31, 33, 34, and 35. To facilitate the prototype manufacture, N_s is selected as 30.

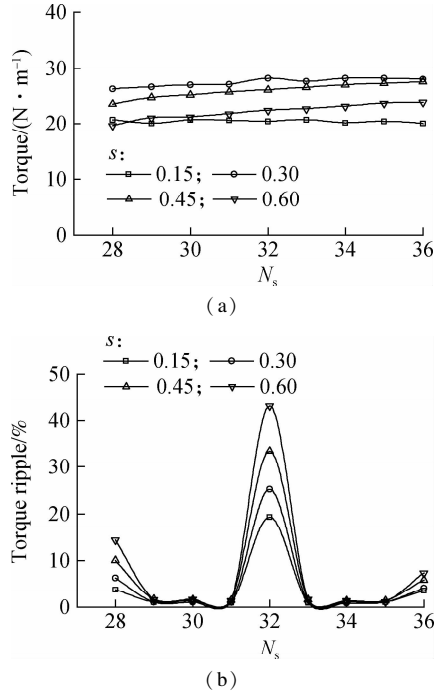

Fig. 8 Torque characteristics of the proposed PMASD (N_s = 28-36). (a) Torque; (b) Torque ripple

4 Experimental Tests

To verify the practical application effects of the scheme, a theoretical prototype was manufactured and tested, which is shown in Fig. 9. A manual control of the MFA was adopted for the principle prototype in this study, while the automatic closed loop control was adopted through an electric actuator for commercialization.

Fig. 10 shows the theoretical speed regulation process of the proposed PMASD with a pump load. The load torque is proportional to the square of the load speed, and

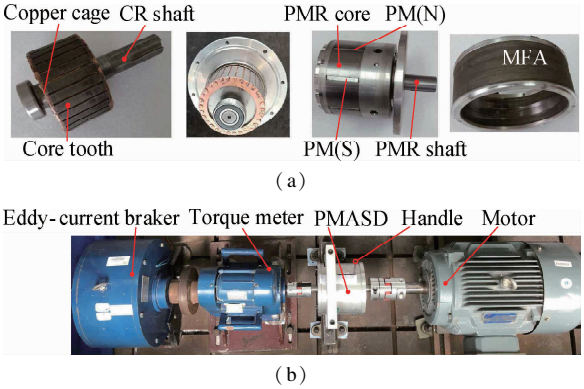

Fig. 9 Prototype and test bench of the proposed PMASD. (a) Main components; (b) Test bench

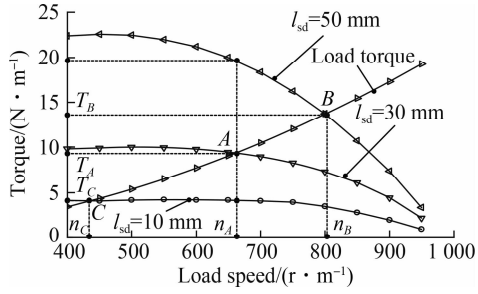

Fig. 10 Speed regulation of the proposed PMASD with a pump load

it gradually increases with the increase in the load speed. Transiently, the driver steadily operates at point A with a load torque T_A and load speed n_A. When a speed-up signal is given, l_{sd} should be enlarged. Assuming that l_{sd} increases to 50 mm, transiently, the torque of the drive increases to T'_A, whereas the load torque keeps T_A. The load speed will rise due to the large T'_A; simultaneously, the load torque gradually increases with the rising load speed. Ultimately, the drive steadily operates at point B with a load speed of n_B when the output torque of the drive is equal to the load torque T_B. Similarly, when a speed-down signal is given, l_{sd} should be decreased. Then, the load speed goes down to n_C at a new steady operation point C when the output torque of the drive is equal to the load torque T_C.

The rated load speed and load torque are set as 800 r/min and 13.68 N · m, respectively. The input power and output power of the drive are shown in Fig. 11. The load torque correspondingly increases with the increase in the load speed. The MFA shifting distance increases from 0 to 50 mm to fit the variable pump load torque. In addition, the speed regulation range reaches 50% compared with the rated output speed. With the increase in the load speed, the copper loss gradually increases, reaches a peak value at approximately 670 r/min, and then gradually declines. The efficiency of the proposed drive linearly increases from 40% to 80% when the load speed goes from 400 to 800 r/min. The input and output powers obtained by the analytical model agree well with the experimental

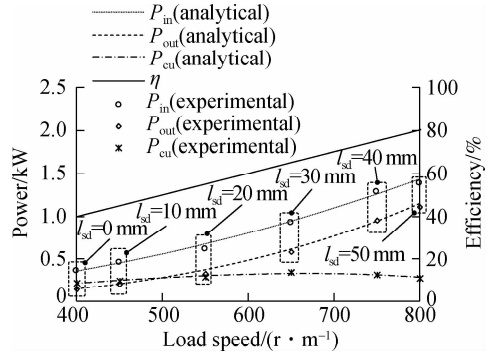

Fig. 11 Power, loss, and efficiency of the proposed PMASD measurement results.

5 Conclusions

1) The output torque increases with the increase in the CR slot number when the copper volume remains unchanged, and the core teeth of the CR are not saturated.

2) The torque ripple is large, and it decreases with the increase in the CR slot number per pole pair (N_{sp}) when N_{sp} is even.

3) The torque ripple is small, and it decreases with the increase in N_{sp} when N_{sp} is odd.

4) The PMASD proposed in this paper has achieved the expected torque transfer and adjustment ability through the prototype test, and the efficient speed regulation and energy saving of the pump and fan system can be realized by the proposed scheme.

References

[1] Xue W L, Tang W, Xu N, et al. Analysis of current situation of energy and electricity consumption and prediction of energy efficiency development during the 14th five-year plan [J]. *Power Demand Side Management*, 2020, **22**(6): 11 – 16. DOI: 10.3969/j.issn.1009-1831.2020.06.003. (in Chinese)

[2] Jitendra S, Binoy K, Krishna M. Innovations in variable frequency drives and its implication in reducing carbon footprint [J]. *Encyclopedia of Renewable and Sustainable Material*, 2020, **3**: 534 – 544. DOI: 10.1016/B978-0-12-803581-8.11010-0.

[3] Zhang C H, Huang K, Xu X M. Application of permanent magnetic speed regulating and variable frequency speed regulating technology in circulating water pump of coal preparation plant [J]. *China Energy and Environmental Protection*, 2018, **40**(2): 144 – 149. DOI: 10.19389/j.cnki.1003-0506.2018.02.029. (in Chinese)

[4] Wallace A, Von Jouanne A. Industrial speed control: Are PM couplings an alternative to VFDs? [J]. *IEEE Industry Applications Magazine*, 2001, **7**(5): 0 – 63. DOI: 10.1109/2943.948533.

[5] Lubin T, Rezzoug A. Steady-state and transient performance of axial-field eddy-current coupling [J]. *IEEE Transactions on Industrial Electronics*, 2015, **62**(4): 2287 – 2296. DOI: 10.1109/TIE.2014.2351785.

[6] Qu Y Q. Application of high-voltage variable-frequency

regulating speed technology in energy saving transformation of thermal power plants [J]. *Energy and Energy Conservation*, 2022, **1**:76 - 78. DOI:10.16643/j.cnki.14-1360/td.2022.01.022. (in Chinese)

[7] Jiao Q F. Research on speed regulation and energy saving transformation of auxiliary circulating water pump [J]. *Energy and energy conservation*, 2017, **2**: 74 - 76. DOI:10.16643/j.cnki.14-1360/td.2017.02.032 (in Chinese)

[8] Zhu Z G. Selection of high-voltage frequency converter and fluid coupler [J]. *Metallurgical Industry Automation*, 2018, **42**(2): 68 - 70. DOI: 10.3969/j.issn.1000-7059.2018.02.015. (in Chinese)

[9] You R, Chai J, Sun X, et al. Variable speed wind turbine based on electromagnetic coupler and its experimental measurement [C]//*Proceedings of* 2014 *IEEE PES Gen Meeting*. National Harbor, MD, USA, 2014: 1 - 5. DOI: 10.1109/PESGM.2014.6939318.

[10] Yang C J, Lu Y G, Li Z B, et al. Finite element analysis of transient air-gap magnetic field for deep bar squirrel cage asynchronous magnetic coupling [J]. *Journal of Jiangsu University* (*Natural Science Edition*), 2012, **33**(2): 193 - 198. DOI: 10.3969/j.issn.1671-7775.2012.02.014. (in Chinese)

[11] Dai X, Liang Q H, Cao J Y, et al. Analytical modeling of axial-flux permanent magnet eddy current couplings with a slotted conductor topology [J]. *IEEE Transactions on Magnetics*, 2016, **52**(2): 1 - 15. DOI: 10.1080/15325008.2015.1070934.

[12] Li Y B, Lin H Y, Tao Q C, et al. Analytical analysis of an adjustable-speed permanent magnet eddy-current coupling with a non-rotary mechanical flux adjuster [J]. *IEEE Transactions on Magnetics*, 2019, **55**(6): 1 - 5. DOI: 10.1109/TMAG.2019.2893458.

[13] Li Y B, Lin H Y, Yang H. A novel squirrel-cage rotor permanent magnet adjustable speed drive with a non-rotary mechanical flux adjuster [J]. *IEEE Transactions on Energy Conversion*, 2020, **36**(2): 1036 - 1044. DOI: 10.1109/TEC.2020.3028881.

[14] Li Y B, Huang J C, Gao F Z, et al. The analytical comparative analysis of electromagnetic characteristics of four typical radial flux permanent magnet eddy current couplers [J]. *Energies*, 2021, **14**(24): 8407. DOI: 10.3390/en14248407.

[15] Hwang S M, Eom J B, Hwang G B, et al. Cogging torque and acoustic noise reduction in permanent magnet motors by teeth pairing [J]. *IEEE Transactions on Magnetics*, 2000, **36**(5): 3144 - 3146. DOI: 10.1109/20.908714.

[16] Li F, Wang K, Gao P W, et al. Investigation of cogging torque and torque ripple in consequent pole permanent magnet machine with different slot/pole number combinations [J]. *Proceedings of the CSEE*, 2022, **42**(17): 6491 - 6498. DOI: 10.13334/j.0258-8013.pcsee.211344. (in Chinese)

气隙固定磁通可调型永磁调速器极槽配合分析

李毅搏[1] 黄家才[1] 朱志莹[2]

([1] 南京工程学院工业中心、创新创业学院, 南京 211167)

([2] 南京工程学院电力工程学院, 南京 211167)

摘要:为了提升永磁调速器的输出转矩,并简化其调速过程中所需机械操动机构,将开槽导体转子结构和机械调磁方法相结合,提出了一种气隙固定磁通可调型永磁调速器. 首先,分析新型永磁调速器的结构特征和运行原理;然后,基于理论模型和有限元法分析影响其基本电磁特性的关键因素,重点研究永磁极数与导体转子槽数之间的配合问题,并获取多种极槽配合情况下输出转矩-滑差特性以及转矩脉动情况;最后,以输出转矩最大、转矩脉动最小为目标,获取最优极槽配合方案,并制造原理样机,得到其调速特性、功率、损耗和效率. 结果表明:每对极导体转子槽数为奇数时,转矩脉动小;每对极导体转子槽数为偶数时,转矩脉动较大,并且随着每对极导体转子槽数的增加,转矩脉动降低.

关键词:永磁调速器;极槽配合;理论模型;有限元方法;笼型转子;转矩特性

中图分类号:TM351